ChemElectroChem

Research Article
doi.org/10.1002/celc.202101617

Chemistry Europe
European Chemical Societies Publishing

www.chemelectrochem.org

Carbon Aerogel Based Thin Electrodes for Zero-Gap all Vanadium Redox Flow Batteries – Quantifying the Factors Leading to Optimum Performance

Andres Parra-Puerto,[a] Javier Rubio-Garcia,[a, b] Matthew Markiewicz,[a, c] Zhuo Zheng,[a] and Anthony Kucernak*[a]

Direct growth of resorcinol–formaldehyde carbon aerogels (CAGs) on carbon paper electrodes was achieved using a new approach. Materials with variations in density, mesoporosity and microporosity were prepared. Microstructural properties of the resultant thin electrodes are shown to directly influence performance in zero-gap redox flow battery (RFB). BET analysis shows a total surface area between 643 to 931 $m^2 g^{-1}$. Deposition of only $\approx$15 wt.% CAG on the carbon electrode leads to a 320-fold increase in electrochemical surface area. Analysis of the results saw a strong positive correlation of RFB performance with surface area. The best performing electrodes had a good balance between microporous and external surface area, and on the macroscopic scale had sufficiently large pores to allow efficient electrolyte permeation. The poorest performing electrodes which had the highest surface area, also had poor macroscopic porosity leading to large mass transport and solution resistance losses. The best performing electrodes were tested in a zero-gap setup using polarization curves, showing a 25% increase in power density at 100 $mA\,cm^{-2}$ and a peak power density of 706 $mW\,cm^{-2}$ at 1 V using thin electrodes.

Introduction

Renewable energies such as solar and wind are playing a key role for decarbonization of the electric sector. However, their intermittency require a large scale energy storage system to supply the electricity into the grid during periods of peak demand.[1] Electrochemical energy storage can play an important role in such applications and have been demonstrated in commercial systems.[2] In this context, redox flow batteries (RFBs) are a promising class of electrochemical storage system due to their ability to scale to medium/large systems, durability, fast response, low maintenance cost and safety.[3] The core of RFBs are the redox species used in liquid or gas form.[4] The vanadium redox couple is the most commonly used to date.[5] All-Vanadium RFBs offer an impressively long calendar and cycling life (around 10 000 cycles in deep discharge) having a relatively low decay in capacity. However, around 54% of the capital cost for a 10 h storage system is the vanadium electrolyte.[6] This cost constraint results in RFB operation at current densities at which the utilization of the electroactive species is maximised. To achieve high performance in RFBs, a number of important parameters need to be considered such as: mass transport, electrode degradation, electrical and ionic conductivity, long-term behaviour. Among them, mass transport limitations associated with electrode porosity, surface area and wettability[3b,5a, 7] are directly associated to achieving a high electrolyte utilization and lower capacity cost. In this context, the development of high surface area and thinner electrodes can have a positive impact reducing the size of the stack in the zero-gap setup.[5b,8] Furthermore, better performing electrodes enable a drop in the total stack cost, as less materials such as bipolar plates or membrane is required for the same power output. On the other hand, using thinner electrodes in flow through systems, may lead to an increase of pressure drop[3a] and decrease of surface area, which can be mitigated by tuning the electrode microstructure.

The most commonly used electrode material in RFBs are polyacrylonitrile (PAN) or pitch-based carbon graphite felts (GFs) due to their chemical stability and low cost.[9]

A number of studies have attempted to modify the properties of the thick GFs in order to improve their properties.[10] Recently Jiang et al. reported a carbon aerogel (CAG) supported on a GF for vanadium RFBs, achieving an increase of 33% in energy efficiency compared with the pristine GF.[11] CAG nanoporous materials are very interesting due to their useful properties such as high surface area and electrical conductivity,[12] and have also been previously used as catalyst support and supercapacitor electrodes materials.[13] However those electrodes still have some limitations including a high areal series resistance (ASR) as relatively thick electrodes are

[a] Dr. A. Parra-Puerto, Dr. J. Rubio-Garcia, Dr. M. Markiewicz, Z. Zheng, Prof. A. Kucernak
Department of Chemistry
Imperial College London
London, SW7 2AZ, UK
E-mail: anthony@imperial.ac.uk

[b] Dr. J. Rubio-Garcia
Current Address: Department of Materials Science & Metallurgy
Cambridge University
Cambridge, CB3 0FS, UK

[c] Dr. M. Markiewicz
Current Address: Ballard Power Systems
Vancouver, 9000 Glenlyon Pkwy, Burnaby, BC V5J 5J8, Canada

ChemElectroChem

Research Article
doi.org/10.1002/celc.202101617

**Chemistry
Europe**
European Chemical
Societies Publishing

required to maximise interfacial (electrochemical) surface area whilst maintaining high porosities. Suitable strategies aimed to improve the volumetric power density of the RFB have been reported relying on replacing the GF with a thinner electrode such as carbon paper (CP),[8] which is more than 20 times thinner, thus reducing the ASR and increasing the power density with reasonable electrolyte utilisation values, however due to the decrease the active surface area, usually 3 layers of CP are used.[14]

Results and Discussion

The aerogel polycondensation of resorcinol-formaldehyde goes through an addition reaction to produce mono- and dimethylol resorcinol.[15] And after, utilising a basic catalyst, the methylol compounds formed goes through a condensation reaction to obtain nanometric clusters, which crosslink, producing the gel. The alkaline catalysts used in the synthesis have a pKb value of 3.67 and -0.5 for the Na_2CO_3 and NaOH respectively.[16] The gelation (cross-linking) time is dependent upon the initial pH of the solution.[13a,15] As investigated by Job et al.[17] the aerogel generated before and after pyrolysis changes from macro-

microporous (isotherm change from type I–II) to microporous (isotherm type I) when the pH is increased in the gelation solution. In our experiments we utilise a similar approach, comparing the effect of the catalyst used during the gelation process, but have taken extra care not to destroy the carbon aerogel structure by using a solvent exchange and freeze-drying process for liquid removal before pyrolysis. The process is described in the experimental section.

Figure 1 shows the SEM and optical microscopy images of the supported CAGs in the carbon paper fibres after pyrolysis under N_2, using the different synthetic parameters where the labels are of the form R/C | R/W. R/C is the resorcinol to catalyst mol ratio (catalyst either NaOH or Na_2CO_3); and R/W is the resorcinol to water mass ratio. In all cases the resorcinol to formaldehyde mol ratio was 0.4. In the SEM images (top) it is possible to observe a different growth of the aerogel (clearer in 1000 | 0.2) using the two catalysts. For both catalysts, when the ratio of resorcinol to catalyst is high, the particles of aerogel tend to be largely associated with a small number of nucleation sites. In contrast, when the R/C ratio is low, the deposition of CAG is much more uniform e.g. a greater dispersity of nucleation points, obtaining a smaller average size of CAG particles. This observation is in accordance with the aerogel
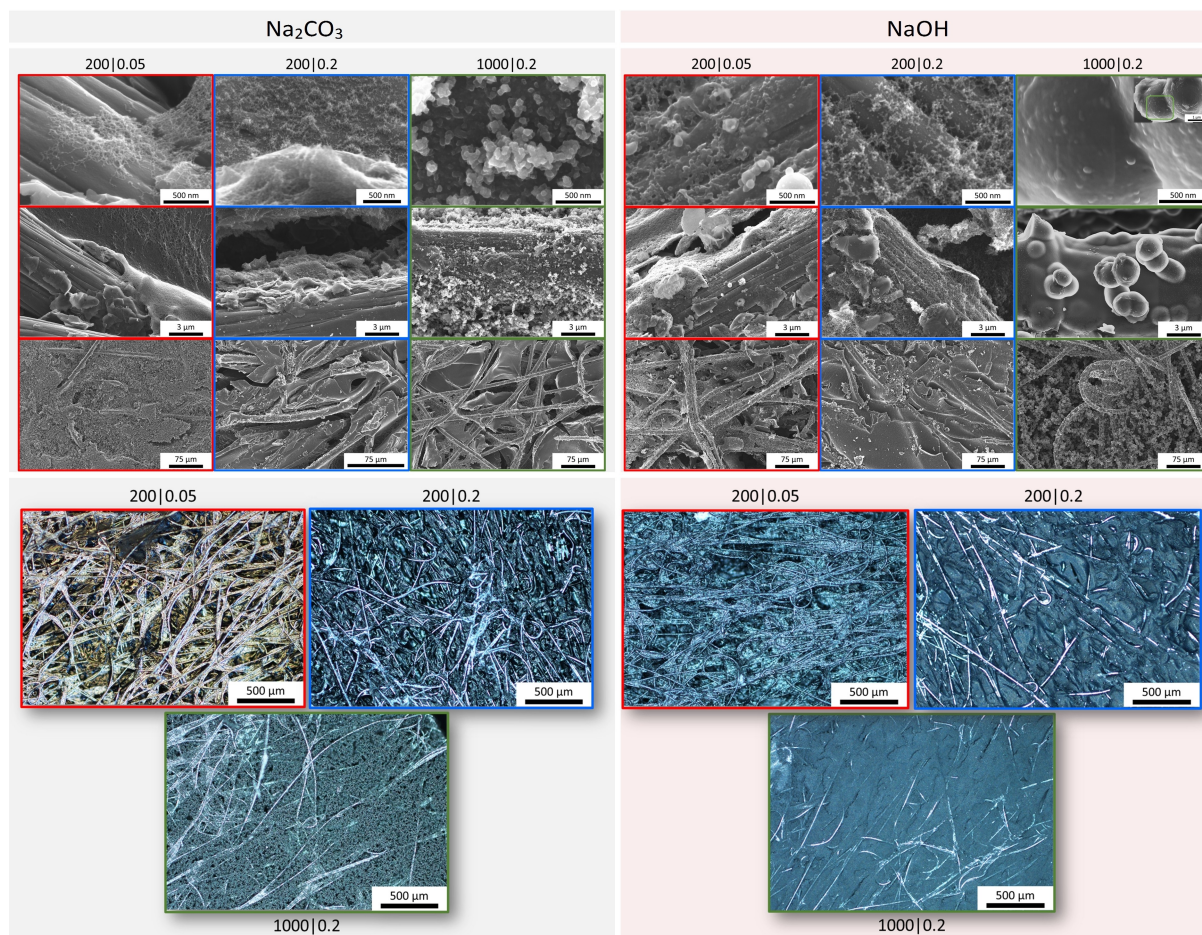

Figure 1. SEM (top) and optical microscopy (bottom) images of the aerogel on carbon paper prepared with the different catalyst ratio and monomer concentration (R/C molar ratio | R/W weight ratios), using Na_2CO_3 (left, light grey) and NaOH (right, light red) as catalyst (inset on the top right, the scale is 1 μm), respectively. R:resorcinol; C:catalyst; W:water.

ChemElectroChem

Research Article
doi.org/10.1002/celc.202101617

**Chemistry
Europe**

European Chemical
Societies Publishing

polymerisation mechanism.[18] Comparing the samples, the largest morphological differences are seen between changes to the R/C ratio (200 to 1000) leading to a macroscopic change in the morphology. A secondary effect is seen with changes in pH as the samples show a very clear difference between Na_2CO_3 and NaOH as catalyst, obtaining a more packed and dense CAGs around the carbon fibres of the electrode support using NaOH, as expected, due to the enhancement in the CAG nucleation with the increase of the pH in the solution.

These effects are also seen at larger distance scales in the optical photomicrographs of the materials (Figure 1, bottom). It is possible to observe a clear difference between those materials made with Na_2CO_3 compared to those made with NaOH. The materials produced with Na_2CO_3 are in general more porous and less dense than the ones prepared with NaOH. Only in the case of the electrode 200|0.05 which looks more similar using both catalysts.

As shown in Figure 2a,d, the isotherms generated are type IV (mesoporous) for 200|0.2 and 200|0.05 using Na_2CO_3 and

NaOH respectively, type IV–II (microporous-mesoporous) for the other R/C=200, and type I for the R/C=1000 (purely microporous), for both catalysts.

Table 1 provides further details of the aerogel powder characteristics, obtained from the modified electrode, as a function of composition of the CAG growth medium and the catalyst (Na_2CO_3: light grey and NaOH: light red). For both catalysts it was observed that gelation did not occur when a low concentration of monomer and/or a low catalyst ratio (e.g. R/C=1000; R/W=0.05) was used. Under the other combinations of R/C and R/W ratios, the gelation and polymerisation of the CAGs on the activated carbon paper electrode were a success. Regardless of the catalyst, when the resorcinol to catalyst ratio is high (1000), the majority of surface area exists in small micropores, and there is little external area. This is because the CAG seems to form somewhat dense structures which preferentially nucleate and grow on the carbon fibres. In contrast, when the resorcinol/catalyst ratio is lower (200), the distribution of surface area micro/mesopore volume is more
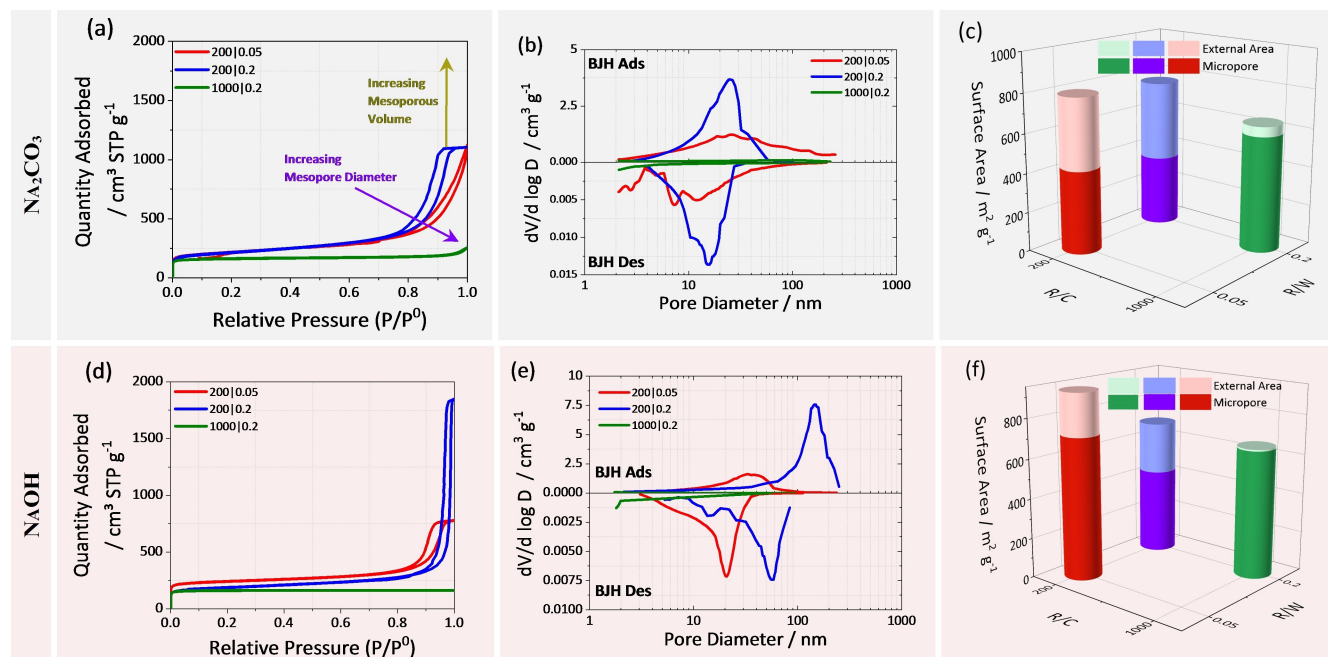

Figure 2. Surface analysis plots of the different aerogels modified with different R/C and R/W ratios. Left column plots, (a,d), N_2 adsorption-desorption isotherms at 77 K. Middle plots, (b,e), pore diameter change distribution of the prepared aerogels. Right column plots, (c,f), surface area with the external and micropores ratios. Na_2CO_3 (light green background) and NaOH (red light background). R:resorcinol; C:catalyst; W:water.

Table 1. CAGs surface properties using different growth mediums for the microstructure modification prepared on carbon paper, the values obtained come from the scratched powder form the electrode prior single cell test (not the electrode with the CAG); S (Surface Area), V (Pore Volume) and D (pore average diameter).

Catalyst	R/C	R/W	S_{BET} $[m^2 g^{-1}]$	Micropore Area [%]	External Area [%]	$V_{Cum. <50 nm}$ $[cm^3 g^{-1}]$	$V_{Micropore}$ $[cm^3 g^{-1}]$	$V_{Mesopore}$ $[cm^3 g^{-1}]$	V_{Micro} [%]	V_{Meso} [%]	D_{avg} [nm]
Na_2CO_3	200	0.05	791.7	47	53	1.324	0.179	1.145	14	86	16.1
	200	0.2	763.5	54	46	1.718	0.154	1.565	9	91	13.9
	1000	0.2	643.2	92	8	0.311	0.229	0.083	73	27	15.3
NaOH	200	0.05	931.1	77	23	1.195	0.280	0.915	23	77	16.8
	200	0.2	689.8	63	37	1.375	0.177	1.198	13	87	42.8
	1000	0.2	655.6	99	1	0.249	0.246	0.003	99	1	2.2

Considering pore size diameter of the Micro(pore) < 2 nm and Meso(pore) between 2 to 50 nm.

ChemElectroChem

Research Article
doi.org/10.1002/celc.202101617

**Chemistry
Europe**
European Chemical
Societies Publishing

balanced and depends on the catalyst used. Pore size distribution during adsorption and desorption are shown in Figure 2b and e, for each deposited material. The CAGs grown using Na_2CO_3 (Figure 2b) as catalyst shows a small shift in the pore size distribution, keeping the peak at the same position. In contrast, using NaOH as catalyst, the pore size distribution and the peak position is shifted, being more affected by the R/W ratio Figure 2e. For both aerogels (200|0.05 and 200|0.2) obtained with Na_2CO_3 (Figure 2b) the pore diameter distribution in the adsorption and desorption processes are quite symmetric in comparison with the ones obtained with NaOH which show asymmetry (Figure 2e).

The 200|0.2 loses its symmetry obtaining different shapes for adsorption and desorption, Figure 2e. This is an indication of the formation of pore necks. Figure 2c and f show the external and micropore areas of the different aerogels. The total surface areas of all samples are quite close to each other, being within 25% of the mean surface area for all the samples. However, there is a significant variation between internal and external surface areas. For the 200|0.05 and 200|0.2 samples the % microporous area is similar although the average value of the ratio depends on the catalyst being about 50% for Na_2CO_3 and 70% for NaOH. In contrast, the 1000|0.2 sample gives close to 100% microporous area, which is correlated with Figure 2a, which shows a high level of microporous structure in the aerogel (Table 1). The effect of the pore size was modelled by Huang et al.[19] for organic and aqueous electrolytes and different pore regimes, mentioning that, for aqueous electrolytes the influence of the micropore materials in energy densities is minimal compared with mesopores. On the other hand, Sillars et al.[20] investigated the influence in the capacitance of aerogels with different pore sizes using ionic liquids (ILs), and concluded that for the optimum capacitance and rate performance the pore size is different, achieving better mass transport with a pore size of around 6.5 nm and the optimal pore size for the capacitance of 4.5 nm.

To understand how the porosity of the CAG thin electrodes influences the electrochemical performance in a thin electrode Zero-Gap RFB setup with only one electrode in each side, all electrodes were tested using the same electrode structure as anode and cathode. The polarization curves were measured with a 100% SoC electrolyte. This is a very useful method to test the electrodes and assess how the CAG structure affects mass transport and ohmic drop as a function of current density.[21] From Figure 3a and b it is clear that the Na_2CO_3 catalyst improves the performance of the RFB compared with the non-modified commercial electrode (SGL SIGRACET 10 AA), whereas when NaOH is used as the catalyst the performance is generally lower than the underivatized carbon paper.

However, all of the aerogels prepared (apart from 1000|0.2| NaOH) show higher performance in the low current region (Current density (j) ≤ 100 mA cm^{-2}) compared to the substrate material, indicating a smaller kinetic overpotential loss associated with higher specific surface area and higher kinetic activity. It is important to note that typically redox flow batteries operate with current densities in the 75–140 mA cm^{-2} range. If we focus on Figure 3a, the activation losses of 200|0.05 and

200|0.2 are small compared to the other two substrates. At high current densities, useful for establishing mass transport and kinetic overpotential effects, these two electrodes achieve a peak power close to 1 V of 562 and 706 mW cm^{-2}, respectively. Both electrodes have quite similar microstructural properties (Table 1), the only difference is that the 200|0.05 electrode has a lower mesopore volume compared with the 200|0.2, giving worse performance in the polarization curve due to mass transport losses, meaning a lower utilization of the electroactive species. However, this electrode has the higher OCP potential suggesting that the mesoporosity plays an important role in the electrocatalytic performance of the vanadium RFB electrode, due to the large solvation radius of the electroactive ions.

This range of pore sizes, not only allows pore flooding with the electrolyte, improving the electrochemically active surface area, but is an advantageous microstructure which enhances the exchange of electroactive species to/from the bulk to the pores.[20] Having a look in the resistance of the electrodes at the different current densities applied, Figure 3c and d, for Na_2CO_3 and NaOH respectively. It is possible to observe that all the CAGs electrodes have lower values of HFR compared with the plain SGL, only in the case of 1000|0.2 using NaOH do we see the higher resistance. The high HFR value for this electrode is possibly due to the nature of the CAG, as it has the smallest pore size and is purely microporous.

Of significant interest is the performance of sample 200|0.2 NaOH, this sample has similar porosity as the Na_2CO_3 samples 200|0.05 and 200|0.2, and also fairly similar to the NaOH sample 200|0.05 but with almost double pore size and a bit more microporous nature (Table 1). In the low current region (current density (j) ≤ 100 mA cm^{-2}) it performs the best of all the NaOH samples and not dissimilar to the 200|0.2 Na_2CO_3. However, at higher currents (current density (j) > 100 mA cm^{-2}) the performance shows a significant drop. Comparing the features of the different samples in Table 1 it is not immediately obvious why the 200|0.2 NaOH sample should perform so poorly at high current densities. The reason for this significant performance drop is revealed by the differential adsorption plots in Figure 2 (e). The 200|0.2 NaOH sample shows a significant hysteresis in these plots indicating that the large pores in the sample are connected by small "necks". Thus, even though the sample might appear to have a good distribution of surface area in reasonably large pores, that surface area is poorly accessible due to the way the pores are interconnected. This means that at high current densities, the "necks" limit mass transport of reactant to a significant proportion of the electrode surface area, leading to a large effective mass-transport loss. In contrast, the electrodes which perform well at high current densities, Na_2CO_3 samples 200|0.05 and 200|0.2 show very symmetrical differential plots (Figure 2 (b)), indicating that access to the high surface area is not hindered by pore "necks". Such a structure is also replicated in the optical microscope images Figure 1: it is possible to notice that the CAG density over the fibres is much greater compared to the analogous in Na_2CO_3 and the 200|0.05 in NaOH, obtaining a more compact layer over the fibres of the carbon paper.
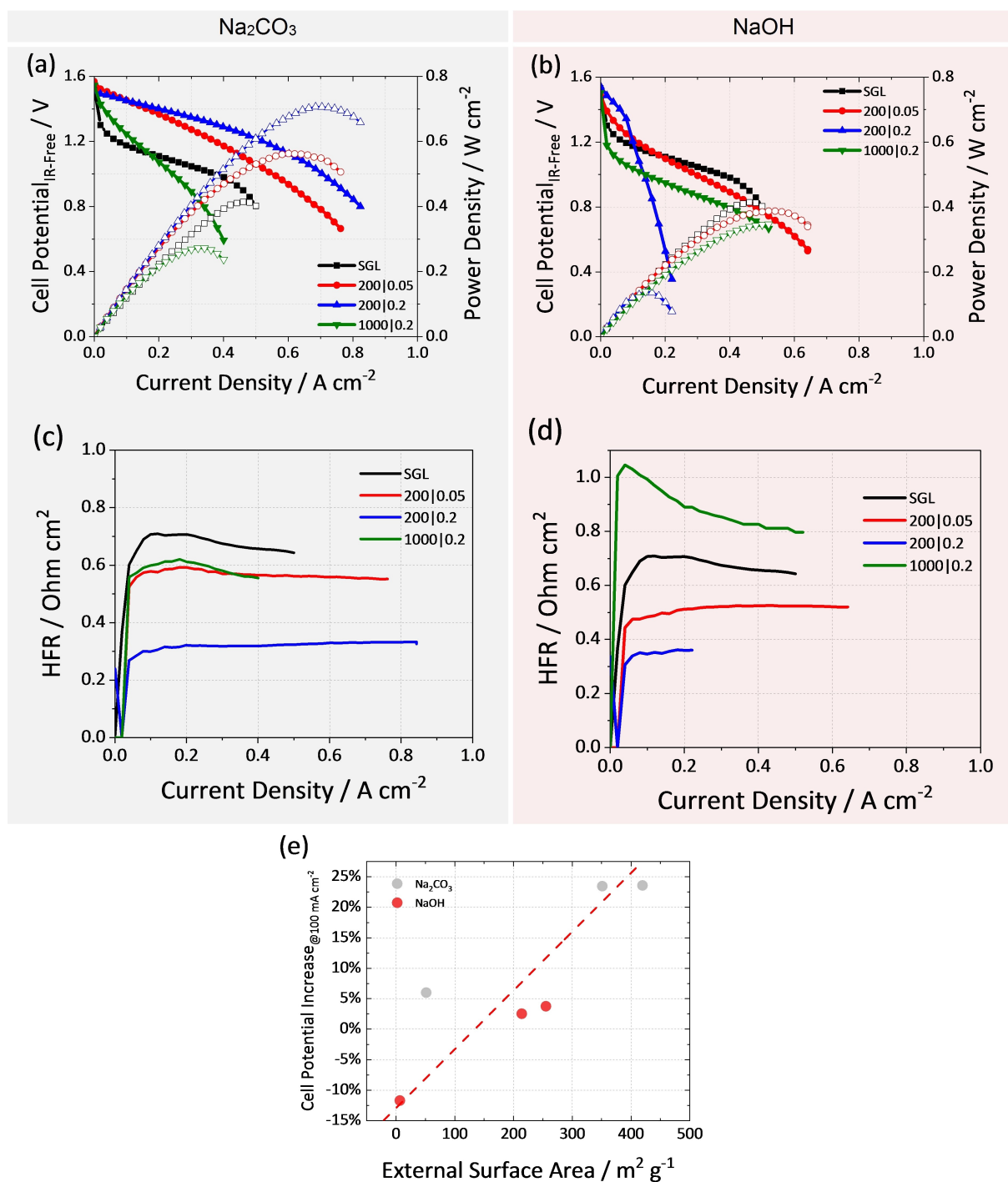
ChemElectroChem

Research Article
doi.org/10.1002/celc.202101617

Chemistry Europe
European Chemical
Societies Publishing

Figure 3. Polarization curves using a zero-gap RFB with one electrode layer in each side of the CAG-CP samples with the different R/C ratios and Na_2CO_3 (a) and NaOH (b) catalyst and the respectively High Frequency Resistance (HFR) (c,d). e) Correlation of improvement in cell potential at a current density of 100 mA cm^{-2} as a function of external surface area. Operating conditions: 300 mL of electrolyte at 100 % SoC, with a current step of 100 mA and holding each point during 10 sec. R:resorcinol; C:catalyst; W:water.

In order to understand which morphological parameters had the biggest effect on performance, the RFB cell potential at a current density of 100 mA cm^{-2} (a common operational performance point) was compared to that on the underivatized carbon electrode as a function of the morphological parameters in Table 1. The strongest correlation was found for the external surface area, Figure 3e. The positive correlation with external surface area suggests that easily accessible surface area is important in achieving good performance at technologically relevant current densities. Increasing the external surface area to 400 m^2 g^{-1} leads to a 25 % improvement in cell voltage.

We have also analysed the cyclic voltammograms (CVs) of the electrodes tested in a three electrode cell using 10 mM V (IV) in 1 M H_2SO_4 solution, Figure S2. Although the CV curves

ChemElectroChem

Research Article
doi.org/10.1002/celc.202101617

**Chemistry
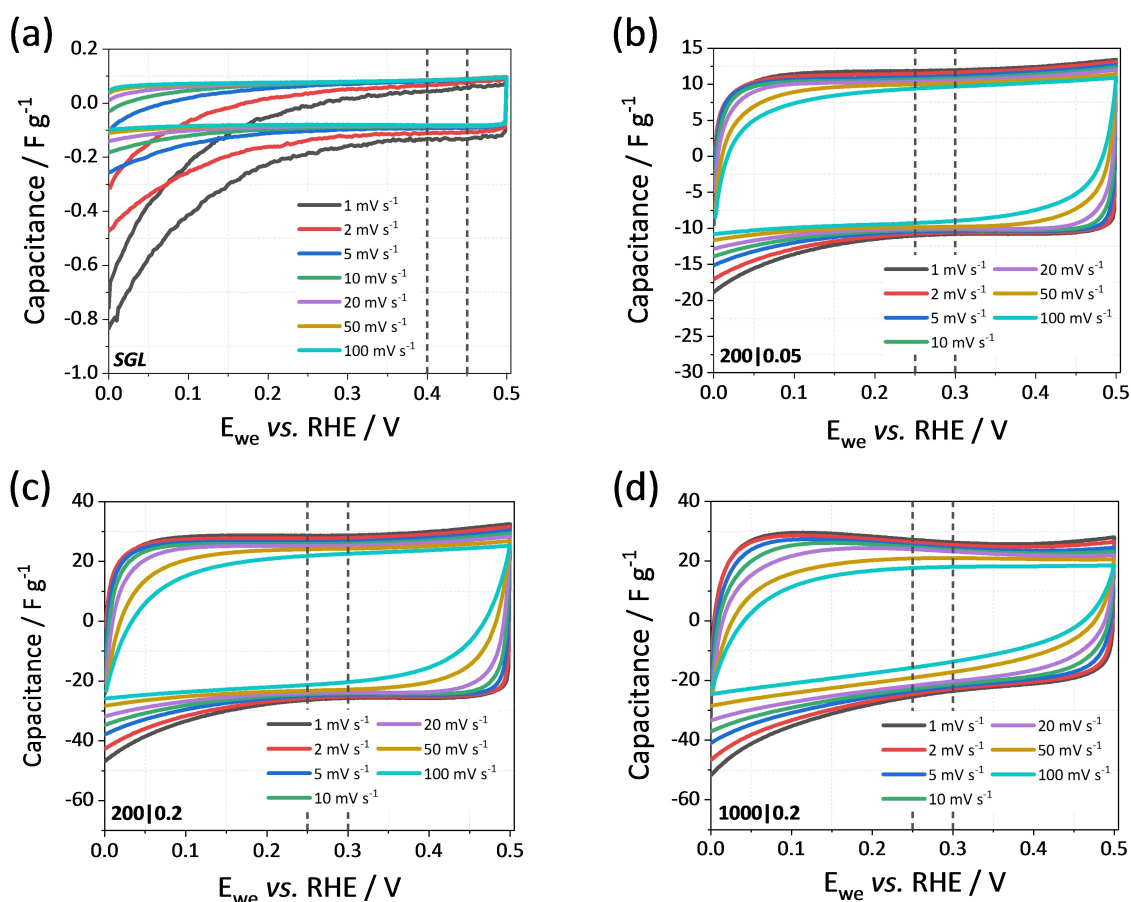Europe**

European Chemical
Societies Publishing

Figure 4. Capacitance measurements at different scan rates (the capacitance is normalised by the scan rate and the total loading) for each electrode prepared with Na_2CO_3: SGL (a), 200|0.05 (b), 200|0.2 (c) and 1000|0.2 (d) with the range of potentials (between dashed lines) used to calculate the average capacitance values for each electrode. (d) Capacitance measurements of the electrodes prepared with the Na_2CO_3 catalyst. At 1 mV s^{-1}, 0.5 M H_2SO_4, purged with N_2 at 298 K.

are modified by the different amounts of capacitance associated with the different electrodes, it is possible to estimate the relative activity of each electrode by monitoring the difference in potential of the oxidation/reduction peaks (ΔE_p) on the respective materials. The ΔE_p values follows the same trend with the performance obtained in the polarization curves at low current densities. The best value is for the 200|0.2|Na_2CO_3 (69 mV), and the second best is for the same composition but in NaOH (75 mV). Although the CVs provide useful information in terms of the catalytic performance of the electrodes, we cannot obtain all the information from the solid electrode structure in the absence of mass transport effects, which instead must be obtained using the polarization curve under the full RFB operating conditions.

To further probe the electrochemical performance of the best performing electrodes produced using Na_2CO_3, double layer capacitance measurements were performed in 0.5 M H_2SO_4 in a three-electrode cell setup at different scan rates. Figure 4, shows the double layer capacitance plots of the different electrodes, normalised by the scan rate and the total electrode weight (shown in Table 2) for each electrode, allowing observation of specific capacitance in the non-Faradaic region.

Table 2. Loading and mass fraction of the different aerogels grown on SGL carbon paper (85 g m^{-2}).

Sample	Mass [g m^{-2}]	CAG Mass Fraction [%]
SGL SIGRACET 10 AA	(85.0)	0
200|0.05	6.2	7
200|0.2	17.6	19
1000|0.2	16.8	18

Figure 4a shows the plain carbon paper electrode (SGL) without any supported CAG, showing at lower scan rates some Faradaic processes possibly associated with electroreduction of small amounts of residual oxygen in solution (note that the y-axis scale is 100-fold smaller than the CAG containing electrodes). Figure 4b, c and d, show the data from the three CAG-based electrodes. There is a significant capacitance increase compared with the plain carbon paper electrode. There are also different degrees of deviation from ideal supercapacitor behaviour, which should look like a square response at all scan rates. Deviations from this form, especially at faster scan rates indicate the presence of ionic (and possibly electronic) transport limitations within the materials leading to internal iR drops and

ChemElectroChem

Research Article
doi.org/10.1002/celc.202101617

Chemistry
Europe
European Chemical
Societies Publishing

limitations to the charging rate. Of the three CAG electrodes, the 200|0.05 and 200|0.2 compositions show the smallest deviation from ideal behaviour at the faster scan rates, whereas the 1000|0.2 shows significant non-ideal behaviour especially at faster scan rates. The significant deviations seen for the latter electrode is not surprising as it is composed almost entirely of micropores (99% by volume, Table 1) with small average pore size (2 nm) and low total internal volume. Hence ion transport within that material is hindered by long transport distances through narrow pores. In contrast the other two materials have much larger internal pore volumes and average pore diameters leading to efficient internal ionic transport.

The values of the capacitance obtained (Table 3) are calculated from the average of the anodic and cathodic charges between the dashed lines (window of 50 mV) in Figure 4 where no Faradic process occurs. Table 3 shows the values obtained from all the electrodes and the CAG alone (subtracting the carbon paper values and considering that each carbon paper used as support gives similar results), to isolate the performance of the different CAGs from the possible support effect.

From the capacitance measurements it is possible to obtain some electrochemical parameters from the electrodes such as the areal and mass specific capacitance of the materials and the electrode roughness factor. Roughness factor (*RF*) denotes the available "real" surface area on which reaction can occur (charge can be stored) relative to the geometric area of the underlying electrode. At higher roughness factors we have an improvement of the electrode surface area and as consequence the electrochemical performance is increased provided other factors such as mass transport and iR drop are not limiting the performance. Electrokinetic performance is increased because although the exchange current density (measured on the specific surface area – i.e. the real surface area) might not change significantly between the CAG and the underlying carbon paper, the available area real surface area increases significantly.

To calculate the different values from the capacitance, shown in Table 3, we use the Equations (1–4).

$$Areal\ Capacitance\ (\text{F m}^{-2}) = \frac{Avg.\ Capacitance\ (\text{F})}{Electrode\ Area\ (\text{m}^2)} \quad (1)$$

$$RF_{\text{BET}} = \frac{SA_{\text{BET}}\ (\text{m}^2\text{g}^{-1}) \times Total\ Weight\ (\text{g})}{Electrode\ Area\ (\text{m}^2)} \quad (2)$$

$$RF_{\text{Capacitance}} = \frac{Avg.\ Capacitance\ (\text{F})}{Electrode\ Area\ (\text{m}^2) \times Specific\ Capacitance_{\text{Carbon}}\ (\text{F m}^{-2})} \quad (3)$$

$$Specific\ Capacitance\ (\text{F g}^{-1}) = \frac{Avg.\ Capacitance\ (\text{F})}{Total\ Weight\ (\text{g})} \quad (4)$$

Where the *Avg. Capacitance* is the value obtained from the potential window between dashed lines in Figure 4, *Area* is the geometric electrode area, *RF* is the roughness factor, obtained from the BET surface area (*SA_BET*) or capacitance, the *Total Weight* is either the weight of CAG or the total weight (CAG plus electrode) of the electrode (Table 2). For comparison, the *RF* determined using BET gas phase surface analysis and in situ capacitance have been calculated. For determining the *RF* using capacitance, we utilise a carbon areal capacitance value of 0.17 F m^{-2}.[22] There is good agreement between the *RF*s determined from BET surface area measurements and capacitance suggesting that all of the surface area seen by BET gas phase measurement is electrochemically accessible.

In the electrodes prepared, it is possible to observe that the roughness factor is dominated by the CAGs which improve the interfacial surface area by a factor of 140–300 (note that although 200|0.05 has a lower roughness factor it also only has a little more than 1/3 as much CAG as the other two electrodes). The highest roughness factor value is observed in the 200|0.2 electrode, providing ample surface area for reaction to occur on, explaining the high performance obtained in the polarization curves (Figure 3). Although the CAG 1000|0.2 electrode has a high *RF*, poor ionic transport through the structure (illustrated in the capacitance plots, Figure 4b) limit RFB performance and does not allow utilisation of the electrochemical surface area due to reactant "starvation" and internal iR drop.

Table 3 also provides the specific capacitance associated with just the CAG material. This is obtainined by subtracting the mass and capacitance of the underlying electrode from the capacitance results. The 200|0.05 CAG gives the highest value 172 F g^{-1} compared with the 1000|0.2 and 200|0.2, which have 134 and 129 F g^{-1}, respectively. In terms of the RFB polarisation curves, 200|0.05 performs better at lower current densities ($j <$ 100 mA cm^{-2}), but is overtaken by 200|0.2 at higher current densities (Figure 3a). In contrast 1000|0.2 performs poorly at all currents, indicating that even though it has a high roughness factor that surface area is all in micropores and hence poorly accessible. This behaviour gives a clear sign that the meso-

Table 3. Electrode and CAG Performance, electrochemical data from the electrode and the CAG extracted from the capacitance measurements and with the pure electrochemical data from the CAGs itself. Surface area Increase relates to the increase in electrochemical surface area associated with the introduction of the CAG. R/C: resorcinol/catalyst mol ratio; R/W: resorcinol/water mass ratio.

Sample	Areal. Capacitance$_{geom}$ [F m^{-2}]	RF$_{BET}$ [m^2 m^{-2}]	RF$_{capacitance}$ [m^2 m^{-2}]	RF Increase Factor	Specific Capacitance (Electrode) [F g^{-1}]	Specific Capacitance (CAG) [F g^{-1}]
SGL	7.4	60	44	(1)	0.1	
CAG 200|0.05	1070	4970	6310	143	11.8	172
CAG 200|0.2	2270	13500	13400	305	22.1	129
CAG 1000|0.2	2260	10900	13300	302	22.2	134

ChemElectroChem

Research Article
doi.org/10.1002/celc.202101617

**Chemistry
Europe**
European Chemical
Societies Publishing

porosity plays a very important role in RFB performance, improving the utilisation of the electrolyte, and as consequence, achieving higher performance. On the other hand, in super-capacitor applications it also plays a role especially under high rates of charge and discharge.

The stability and cyclability of the electrode with the best microstructure and highest performance, was tested using galvanostatic charge and discharge experiments. Figure 5a shows one cycle of charge and discharge obtained at different current densities (50 and 75 mA cm^{-2}). Operation at higher current density leads to lower specific capacity due to a greater mass transport overpotential, and hence, lower electrolyte utilization. The discharge capacity values were 56 and 89% of the theoretical value (13.4 Ah L^{-1}) at 75 and 50 mA cm^{-2}, respectively. This implies higher achievable State of Charge (SoC) and a more efficient utilization of the expensive electrolyte.

Commercially available all-vanadium RFBs are normally operated below 120 mA cm^{-2} (commonly 80 mA cm^{-2}) to ensure high energy efficiency ($\approx 85\%$) and good electrolyte utilization ($> 75\%$).[3a] Figure 5b shows figures of merit associated with the continuous short operation of the all-vanadium RFB during a 20-cycle test. High Coulombic Efficiency of about 90% (CE, ratio of the discharge capacity over the charge capacity) was found which strongly suggest a minimal absence of reactions such as the formation of CO$_2$ by oxidation of the carbon aerogel

structure. Similarly, high Voltage Efficiency (VE, ratio between the average voltage for charging and discharging) was found at relatively large current density (VE $> 85\%$). It is worth mentioning that the pristine carbon paper electrode cannot be operated at such a high current densities.[8] This supports the benefits of tuning electrode porosity and microstructure to enhance the available surface and diminish mass transport limitations which would affect VE. The Energy Efficiency (EE) which is obtained using this system was 75% at 75 mA cm^{-2}, having a comparable EE value to commercial all-vanadium systems which have been optimised for many years.[23] However, it needs to be noticed that large variability in the efficiency is observed in each cycle. We attribute this to the mechanical stability of the aerogel structure which leads to stress and detachment under hydro-dynamic conditions. This is supported by the observation of a small amount of carbon particles at the electrolyte outlet which would contribute to increased mass transport limitations. Gradual electrode degradation is observed after the 11th cycle, in which a gradual decrease of VE is observed even at 50 mA cm^{-2}, the degradation of the electrode 200|0.2 can be observed in Figure S1, if we compare with the fresh sample in Figure 1.

There is a desire to move to such zero-gap systems using thin electrodes as such systems reduce stack size, decrease ionic and electronic iR drop and reduce total system cost. The standard electrode used, graphite felt, has an average thickness of 4.6 mm. On the other hand, in thin electrode zero-gap systems, as the membrane electrode assembly uses thinner electrodes such as carbon papers or carbon cloths (with thicknesses between 0.1 to 0.4 mm), though typically 3-layers of these materials are required in order to achieve a sufficiently high roughness factor. To provide a suitable metric for comparing state of the art RFB electrodes to the current materials used, we need to consider the difference in the electrode thicknesses as this will affect the volumetric performance of the RFB. As a value of merit for the polarization curves, we took the geometric power density at 1 V. With the values obtained of the power density and the volume of the electrodes, we can calculate the volumetric power density (VPD), and for our best performing electrodes a VPD of 14 and 17.7 W cm^{-3} was achieved. To put these values in contect, we compared our values of VPD, and the discharge capacity achieved at specific current densities with those determined for different reported works (Figure 6). This type of plot is a useful way to compare both the dynamic power performance with the ability to utilise all of the electrolyte in an RFB.

Better overall performance for an RFB is achieved by moving to the upper right-hand corner (high volumetric power and large discharge capacity) in Figure 6. Our electrodes show the highest performance for the systems we have been able to characterise from available literature sources. The works included in the diagram are the ones which show both tests, however, in the SI there are more works in which only either the polarization curves or the charge and discharge profiles are provided. Furthermore, many of the results showing the best performance in Figure 6 and in the SI, were assembled with thinner Nafion membranes, typically 25 to 50 μm, which are
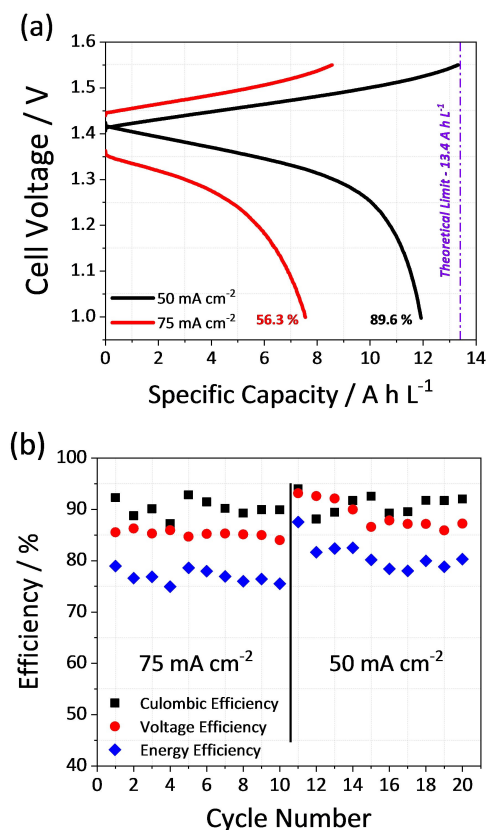

Figure 5. a) Galvanostatic charge and discharge curves at 50 and 75 mA cm^{-2}. b) Battery efficiencies over 20 cycles of charge and discharge at two current densities applied (10 each) using the 200|0.2 electrode.

ChemElectroChem

Research Article
doi.org/10.1002/celc.202101617

Chemistry Europe
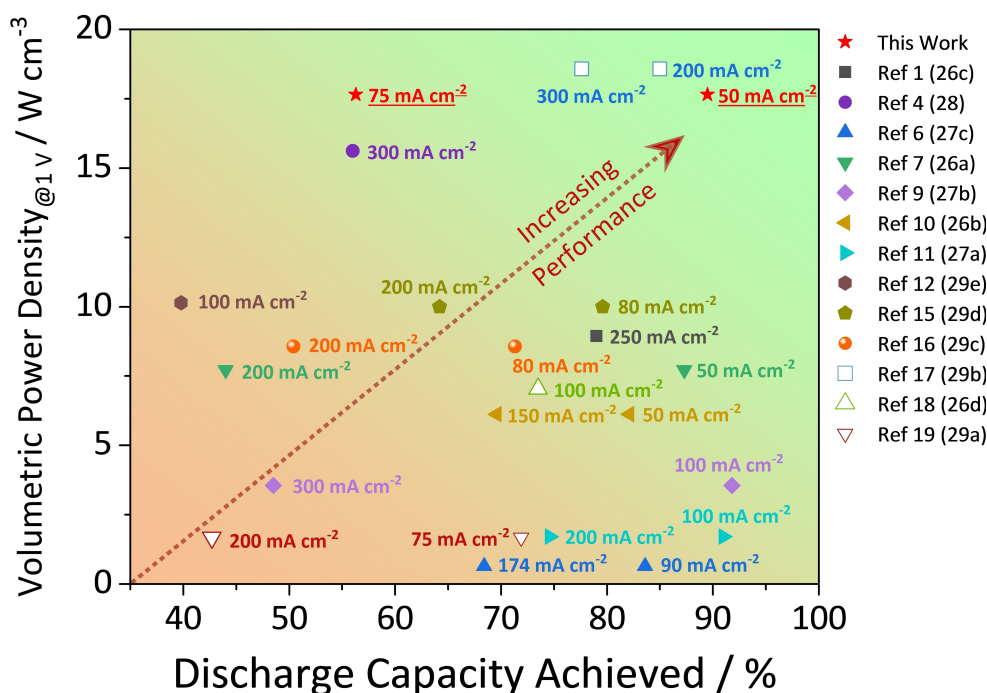European Chemical
Societies Publishing

Figure 6. Comparison of the results obtained without electrode (★) to those obtained in the literature using the volumetric power density obtained from the polarization curves at 1 V and the discharge capacity from the charge-discharge profiles at different fixed current densities. The references naming used is from the SI. Electrode types used in the figure: CP type,[24] GF type,[25] CC (we assumed the thickness to be 0.4 mm, the work did not mention),[26] Electrospun Electrode.[27]

typically not used in real vanadium flow battery systems because of enhanced crossover, but which achieve higher relative performance, whereas in this work we have used a relevant electrolyte thickness (183 μm). Considering this aspect, we observe that our work, using a thicker membrane achieves a very high VPD. On the other hand, some works showed the performance using thinner membranes and similar electrodes thickness as ours,[28] or thinner electrodes and even thinner membranes,[29] which achieve VPD values of 35 and 40 W cm^{-3}, respectively. However, in these works the authors did not report the charge and discharge profiles for the cell setup used in the polarization curves and in any case, these membrane thicknesses, as mentioned above, are not applicable to real systems due to increased rates of vanadium crossover. On the other hand, other reported works, using similar types of CAGs as ours deposited on graphite felt electrode as a substrate,[11] and other using a dual scale porous electrode[30] (based on carbon paper) with very similar thickness as the ones used in this work, do not show the polarization curve for the electrodes tested.

Reviewing the different reported works, the future work needs to be focused on the optimisation of the electrolyte flow rate, as well in the improvement of electrode mechanical properties and long term cyclability at higher current densities, which could enable the application of the materials here presented in real system with sufficient longevity, as well the possibility to growth CAGs in even thinner electrodes to further improve the performance. On the other hand, the synthetic process time to growth the CAGs need to be reduced, to have the possibility to be applied in real systems.

Conclusion

We found that the aerogel micro-structure can be easily tuned by changing the synthesis conditions, the catalyst content gives change in the particle size and the monomer content the affect the loading and mesoporosity of the material. To improve the growth of the CAG over the carbon paper electrode, a plasma treatment under O_2 plasma was performed in order to decrease the hydrophobicity. Two basic catalysts were studied, Na_2CO_3 and NaOH, increasing the pH in the solution when the NaOH is used as catalyst leads to a more compact and denser aerogel. In the case of the Na_2CO_3 catalyst, a more porous layer was obtained with a major mesoporosity contribution using the lower R/C ratio.

The performance obtained from the polarization curves showed that the electrodes prepared using Na_2CO_3 had the best performance, and particularly the electrode 200|0.2, which is the best performing one, obtaining a power density of 706 mW cm^{-2} (17.7 W cm^{-3}).

To get a better understanding of the electrochemical behaviour of the best performing electrodes, capacitance measurements were done for the electrodes prepared using Na_2CO_3. Upon incorporation of carbon aerogels, the electrode roughness factor (and thus interfacial surface area available for reaction) was increased drastically by a factor of 140–300 with respect to the underlying carbon paper. The values of the roughness factor were obtained using both BET and capacitance, having a slightly higher value using the second method using literature values of the specific capacitance of carbon

ChemElectroChem

Research Article
doi.org/10.1002/celc.202101617

Chemistry
Europe
European Chemical
Societies Publishing

electrodes. Considering this structure also, it can lead to more ideal supercapacitor behaviour due efficient ionic transport within the material. On the other hand, it was found that just having high surface area is not enough to achieve high performing RFB electrodes. Instead, the mesoporosity needs to be tailored to allow fast transport of reactants and ions into the structure. Indeed, in the "thin electrode zero-gap setup" RFBs operating at technologically relevant current densities a positive correlation with external surface area is found – i.e. micro-porous surface area does not appreciably contribute to RFB performance.

Testing the best electrode during repeated RFB charge and discharge tests achieved 56% and 90% of the theoretical capacity with an energy efficiency of $>75\%$ at the two different current densities.

In summary, the growth of CAGs in the carbon paper electrode improves the performance of the RFB in almost all cases at low current densities compared to the underivatized carbon electrode. However, to get a good RFB performance the CAG requires good mesoporosity and good pore structures with an absence of "necks" between the mesopores; so, the high surface area material can be accessed by the electrolyte, otherwise the RFB will starve and there will be rapid performance loss at higher currents. Hence, it is not enough to have a high surface area; the porosity must show a suitable hierarchical ordering so that the electrolyte can flow through the structure. This mesoporosity will also affect the pressure drop through the RFB, which has not been studied in this paper with the long term cycling stability, but would be useful in follow up studies.

Improving the surface area to use only one layer of the CAG-CP in each side, it is possible to decrease the thickness of the MEA by an order of magnitude (assuming the same membrane, Nafion 117, is used) from 9.38 mm using GF MEA to 0.99 mm with the CAG-CP MEA. As a consequence, decreasing the volume of the stack by almost a factor of ~3 (assuming 3 mm thick bipolar plates) maintaining the same power density, or having the possibility of increasing the volumetric power density of the stack by a factor of three. Even using a quite low current density for the charge/discharge tests, we obtain a high performance in terms of volumetric power density and electrolyte utilisation. However, more tests need to be performed to increase the current densities value for the charge/discharge tests.

Experimental Section

Carbon Aerogel Electrode Preparation

Hydrogels were synthesized by a previously reported base catalysed polycondensation of resorcinol and formaldehyde.[11] As an example; 6.7 mL of 37% formaldehyde solution (Sigma Aldrich, ACS Reagent, 37 wt.% in water) was diluted with 10.8 mL of water (Millipore Milli-Q, 18.2 MΩ cm), and then 4 g of resorcinol (Alfa Aesar, 99%) was added. The solution was stirred at room temperature until the resorcinol was fully dissolved. Then 2.6 mL of 1.5 g L^{-1} Na$_2$CO$_{3(aq)}$ (VWR) was added (as catalyst), giving a final composition of 1:2.5 molar ratio of resorcinol: formaldehyde (R/F =

0.4, fixed for all experiments in this paper), 1:5 (0.2) mass ratio of resorcinol: solvent, and 1000:1 molar ratio of resorcinol: catalyst (Na$_2$CO$_3$ and NaOH). The different electrodes were named as 200│0.05, 200│0.2 and 1000│0.2 (R/C molar ratio │R/W weight ratio). SGL Carbon Paper (0.4 mm thickness SIGRACET 10 AA with a specific surface area = 0.7 m^{2}g^{-1}, areal weight = 85 g m^{-2}) was first treated with an oxygen plasma to render the material hydrophilic and ensure infiltration by the resorcinol – formaldehyde solution. This activation was performed in a Diener Nano 40 kHz plasma chamber, at 0.3 mBar oxygen pressure (BOC, N5.5) and 300 W plasma power for 10 mins, flipping over the electrode halfway through the process. The activated carbon paper (3×3 cm) was place in a heat-seal bag (NIP30PE75, Skultuna Flexible) filled with 20 mL of resorcinol-formaldehyde solution. The bag was then sealed to avoid solvent evaporation and aged at 90 °C in a convection oven for 7 days at 90 °C. This process formed the hydrogel and allowed impregnation into the carbon paper substrate.

Excess hydrogel was removed from the surface of the carbon paper using a scalpel. This excess material underwent the same work-up as the aerogel loaded carbon paper described below, producing samples of the unsupported material for characterization (scheme of the process is shown in Figure 7).

During the formation of the CAG it is important that micro and meso and macro-pores are not collapsed due to capillary forces. In order to avoid formation of a liquid gas interface (and thus avoid the forces leading to capillary collapse of the structure), we replace the reactant water with tert-butanol which has a low density change on freezing (0.8%), relatively high freezing point of 25.6 °C and thus is ideal as a liquid to use during the freeze-drying process. To remove the soluble impurities, such as the base catalyst and excess formaldehyde, the impregnated carbon paper was soaked in water at 90 °C for 5 days, replacing the solvent with fresh water every 24 h. The solvent was then exchanged with tert-butanol (Sigma-Aldrich, ACS Reagent) at 40 °C for 5 days, exchanging the solvent every 24 h. Finally, an aerogel was formed from the hydrogel by freeze-drying (Christ Alpha 2-4 LD Plus) at 0.01 mBar and −88 °C during at least 72 h.

Aerogels were pyrolyzed in a tube furnace (CARBOLITE MTF 12/38/400) under a flow of nitrogen (BOC, Research Grade). Freshly dried aerogels were loaded into the furnace at room temperature. The furnace was ramped from room temperature to 1000 °C with a ramp rate of 1 °C min^{-1}, dwelled for 8 h at 1000 °C. The furnace was then turned off and allowed to cool to room temperature without forced cooling under N$_2$ Flow (taking ca. 6 hours). The pyrolyzed aerogels were then removed whereby exposing them to air and cut to the appropriate size for further use. The typical loading of the aerogel on each electrode was determined by mass difference from the underivatized carbon electrode, shown in Table 2.

The structural properties of the aerogel were varied by modifying the resorcinol: catalyst molar ratio (R/C) and resorcinol: solvent mass ratio (R/W), summarised in Table 3.

BET and Pore Size Distributions

Surface area and pore size distribution were determined via gas adsorption (TriStar II-Plus surface area and porosity analyser, Micromeritics). Bulk aerogel samples were first ground with a mortar and pestle, and then 100 mg of sample was analysed. For aerogels loaded onto carbon paper, approximately 5 cm^2 of the prepared substrate was analysed. Prior to analysis, samples were dried at 300 °C under a stream of N$_2$ (Air Products, BIP-Plus) overnight, cooled to room temperature, and then evacuated within the instrument for 1 h.

ChemElectroChem

Research Article
doi.org/10.1002/celc.202101617

**Chemistry
Europe**

European Chemical
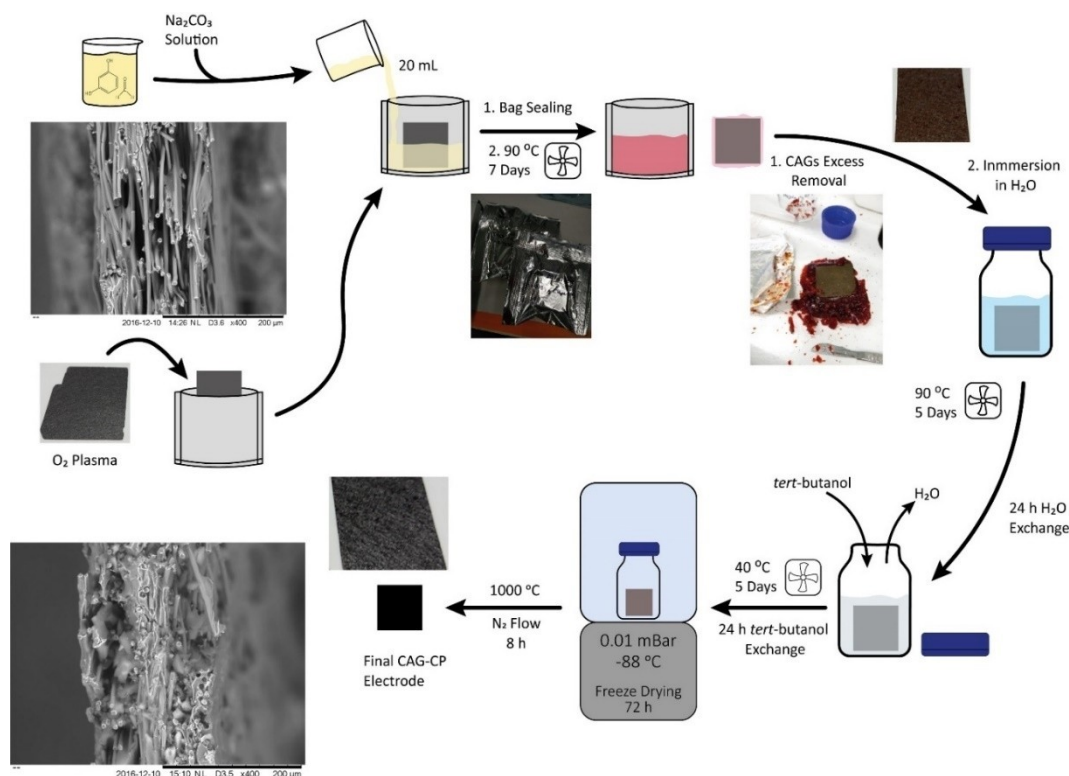Societies Publishing

Figure 7. Scheme of the CAGs synthetic process and a cross section of the carbon paper plain and CAG loaded.

Nitrogen adsorption isotherms were collected for all aerogel samples at liquid nitrogen temperature, while krypton was used as adsorbate for pristine carbon paper due to its low surface area. Mass specific surface areas were calculated using the Brunauer-Emmett-Teller equation within MicroActive, while external and micropore surface area were calculated using the t-plot method. Barrett-Joyner-Halenda (BJH) Pore Size and Volume Analysis was performed on the data in the same software. The total cumulative pore volume was obtained from the cumulative volume of desorbed nitrogen for pore diameters equal or below 50 nm (micro and mesopores).

Physical Characterization

A Hitachi TM3030 table-top SEM was used to obtain the surface images of the different aerogels shown in the SI and a Zeiss LEO Gemini SEM was used for the main paper. An optical microscope Nikon Eclipse LV100D was used to obtain the images of the different aerogels.

Cell Assembly and Electrochemical Characterization

A redox flow battery fixture (Scribner Associates Inc.) of 5 cm^2 with an interdigitated flow field, utilising the same electrode on both sides, was used. Nafion 117 (0.183 mm, Fuel Cell Store) was used as membrane and as gaskets, incompressible glass reinforced PTFE gaskets (Tygaflor) were chosen to provide a 25–30% compression of the electrodes, this means that the electrodes were compressed to 70–75% of the original thickness, considering 0.4 mm as the original thickness the final values used in the polarization curves and cycling tests were between 0.28–0.3 mm.[31] All the electrochemical single cell tests were performed using a 857 Redox Flow Cell Test System (Scribner Associates Inc.).

The electrolyte for the RFB test was prepared by dissolving $VOSO_4 \cdot 4H_2O$ (Alfa Aesar, 98%) to a concentration of 1 M in 3 M H_2SO_4 (VWR, 95% AnalaR NORMAPUR®) utilising ultrapure water (Millipore MilliQ, 18.2 MΩ cm) as solvent. The anolyte and catholyte were prepared electrochemically from VO^{2+}. The catholyte volume was double (60 mL) that of the anolyte (30 mL), and then the total catholyte volume was fully oxidised to VO_2^+ during which process the anolyte is reduced to V^{2+},(under N_2 to avoid the V^{2+} oxidation with air). For the battery cycling tests, the volume of the catholyte and anolyte was equal (30 mL each side).[32] On the other hand, the polarization curves used 300 mL at 100% SoC with a liquid flow of 25 mL min^{-1} to minimise the effect of the recirculation setup and approach close to a single pass setup.

Capacitance measurements were performed in a three-electrode glass cell system using a GAMRY 600 potentiostat, in 0.5 M H_2SO_4 with a Pt mesh as counter electrode and a home-made RHE as reference electrode. The working electrode (1.25 cm^2) utilised a home-made holder (PTFE) to clamp the solid electrode utilising a gold wire used as contact.

The CVs obtained from the electrodes prepared and shown in Figure S2, were done using the same glass cell as in the capacitance measurements, but the potentiostat used was an Autolab (PGSTAT302N) from Metrohm, the solid electrode as reference electrode, a Pt wire as counter electrode and a calomel electrode (SCE) as reference, all the potentials were converted to RHE. The electrolyte was 10 mV of VO^{2+} in 1 M H_2SO_4.

CRediT Authorship Contribution Statement

Andres Parra-Puerto: Formal analysis, Data Curation, Conceptualization, Original Draft, Visualization, Writing - Review & Editing.

State of the Art Reviewing and Summarising. **Javier Rubio-Garcia**: Methodology, Conceptualization, Supervision, Writing - Review & Editing. **Matthew Markiewicz**: Investigation, Data Curation, Methodology, Supervision, Formal analysis, Validation. **Zhuo Zheng**: Investigation, Validation. **Anthony Kucernak**: Conceptualization, Supervision, Data Curation, Project administration, Funding acquisition, Writing – Review & Editing.

Data Availability

The data used in the production of the figures in this paper are available for download at DOI:10.5281/zenodo.6261512.

Conflict of Interest

The authors declare no conflict of interest.

Data Availability Statement

Data will be made available at proofing stage. A data access statement is provided in the paper: "The data used in the production of the figures in this paper are available for download at DOI:10.5281/zenodo.6261512."

[1] B. Dunn, H. Kamath, J.-M. Tarascon, *Science* **2011**, *334*, 928–935.

[2] S. Chu, A. Majumdar, *Nature* **2012**, *488*, 294–303.

[3] a) K. Lourenssen, J. Williams, F. Ahmadpour, R. Clemmer, S. Tasnim, *J. Energy Storage* **2019**, *25*, 100844–100844; b) M. Skyllas-Kazacos, M. H. Chakrabarti, S. A. Hajimolana, F. S. Mjalli, M. Saleem, *J. Electrochem. Soc.* **2011**, *158*, R55-R55.

[4] J. Rubio-Garcia, A. Kucernak, D. Zhao, D. Li, K. Fahy, V. Yufit, N. Brandon, M. Gomez-Gonzalez, *Journal of Physics: Energy* **2018**, *1*, 015006–015006.

[5] a) W. Wang, Q. Luo, B. Li, X. Wei, L. Li, Z. Yang, *Adv. Funct. Mater.* **2013**, *23*, 970–986; b) P. Alotto, M. Guarnieri, F. Moro, *Renewable Sustainable Energy Rev.* **2014**, *29*, 325–335.

[6] L. Joerissen, J. Garche, C. Fabjan, G. Tomazic, *J. Power Sources* **2004**, *127*, 98–104.

[7] a) I. Streeter, G. G. Wildgoose, L. Shao, R. G. Compton, *Sens. Actuators B* **2008**, *133*, 462–466; b) K. R. Ward, R. G. Compton, *J. Electroanal. Chem.* **2014**, *724*, 43–47; c) E. O. Barnes, X. Chen, P. Li, R. G. Compton, *J. Electroanal. Chem.* **2014**, *720–721*, 92–100; d) F. Tariq, J. Rubio-Garcia, V.

[8] Yufit, A. Bertei, B. K. Chakrabarti, A. Kucernak, N. Brandon, *Sustain. Energy Fuels* **2018**, *2*, 2068–2080.

[8] D. S. Aaron, Q. Liu, Z. Tang, G. M. Grim, A. B. Papandrew, A. Turhan, T. A. Zawodzinski, M. M. Mench, *J. Power Sources* **2012**, *206*, 450–453.

[9] S. Zhong, C. Padeste, M. Kazacos, M. Skyllas-Kazacos, *J. Power Sources* **1993**, *45*, 29–41.

[10] a) B. Sun, M. Skyllas-Kazacos, *Electrochim. Acta* **1992**, *37*, 2459–2465; b) B. Sun, M. Skyllas-Kazacos, *Electrochim. Acta* **1992**, *37*, 1253–1260; c) W. H. Wang, X. D. Wang, *Electrochim. Acta* **2007**, *52*, 6755–6762; d) Z. González, C. Botas, P. Álvarez, S. Roldán, C. Blanco, R. Santamaría, M. Granda, R. Menéndez, *Carbon* **2012**, *50*, 828–834.

[11] F. Jiang, Z. He, D. Guo, X. Zhou, *J. Power Sources* **2019**, *440*, 227114–227114.

[12] A. M. Elkhatat, S. A. Al-Muhtaseb, *Adv. Mater.* **2011**, *23*, 2887–2903.

[13] a) M. Ciszewski, E. Szatkowska, A. Koszorek, *J. Electron. Mater.* **2017**, *46*, 4612–4617; b) C. Moreno-Castilla, F. J. Maldonado-Hódar, *Carbon* **2005**, *43*, 455–465.

[14] I. Mayrhuber, C. R. Dennison, V. Kalra, E. C. Kumbur, *J. Power Sources* **2014**, *260*, 251–258.

[15] R. B. Durairaj, *Resorcinol, Chemistry, Technology and Applications | Raj B. Durairaj | Springer*, 1 ed., Springer-Verlag Berlin Heidelberg, New York, **2005**.

[16] W. M. Haynes, *Handbok of Chemistry and Physics. 99th Edition, Vol. 94*, **2018**.

[17] N. Job, R. Pirard, J. Marien, J. P. Pirard, *Carbon* **2004**, *42*, 619–628.

[18] W. Li, G. Reichenauer, J. Fricke, *Carbon* **2002**, *40*, 2955–2959.

[19] J. Huang, B. G. G. Sumpter, V. Meunier, *Chem. Eur. J.* **2008**, *14*, 6614–6626.

[20] F. B. Sillars, S. I. Fletcher, M. Mirzaeian, P. J. Hall, *Energy Environ. Sci.* **2011**, *4*, 695–706.

[21] D. Aaron, Z. Tang, A. B. Papandrew, T. A. Zawodzinski, *J. Appl. Electrochem.* **2011**, *41*, 1175–1182.

[22] a) T. A. Centeno, F. Stoeckli, *J. Power Sources* **2006**, *154*, 314–320; b) C. C. L. McCrory, S. Jung, J. C. Peters, T. F. Jaramillo, *J. Am. Chem. Soc.* **2013**, *135*, 16977–16987.

[23] E. Sánchez-Díez, E. Ventosa, M. Guarnieri, A. Trovò, C. Flox, R. Marcilla, F. Soavi, P. Mazur, E. Aranzabe, R. Ferret, *J. Power Sources* **2021**, *481*, 228804–228804.

[24] a) K. V. Greco, A. Forner-Cuenca, A. Mularczyk, J. Eller, F. R. Brushett, *ACS Appl. Mater. Interfaces* **2018**, *10*, 44430–44442; b) S. Abbas, S. Mehboob, H.-J. Shin, O. H. Han, H. Y. Ha, *Chem. Eng. J.* **2019**, *378*, 122190–122190; c) J. Houser, A. Pezeshki, J. T. Clement, D. Aaron, M. M. Mench, *J. Power Sources* **2017**, *351*, 96–105; d) M. Raja, H. Khan, S. Sankarasubramanian, D. Sonawat, V. Ramani, K. Ramanujam, *Catal. Today* **2021**, *370*, 181–188.

[25] a) S. Bellani, L. Najafi, M. Prato, R. Oropesa-Nunez, B. Martin-Garcia, L. Gagliani, E. Mantero, L. Marasco, G. Bianca, M. I. Zappia, C. Demirci, S. Olivotto, G. Mariucci, V. Pellegrini, M. Schiavetti, F. Bonaccorso, *Chem. Mater.* **2021**, *33*, 4106–4121; b) R. Wang, Y. Li, H. Liu, Y.-L. He, M. Hao, *J. Mater. Chem. A* **2021**, *9*, 2345–2356; cT. Davies, J. Tummino, *C* **2018**, *4*.

[26] H. Ishitobi, S. Yamamoto, T. Ishii, K. Oba, H. Doki, R. Obata, A. Miyashita, H. Okazaki, N. Nakagawa, *J. Chem. Eng. Jpn.* **2021**, *54*, 219–225.

[27] a) M. Jing, X. Qi, X. An, X. Ma, D. Fang, X. Fan, J. Liu, C. Yan, *Electrochim. Acta* **2021**, *390*; b) J. Sun, H. Jiang, C. Zhao, X. Fan, C. Chao, T. Zhao, *Sci. Bull.* **2021**, *66*, 904–913; c) J. Sun, H. R. Jiang, M. C. Wu, X. Z. Fan, C. Y. H. Chao, T. S. Zhao, *J. Power Sources* **2020**, *470*; d) J. Sun, L. Zeng, H. R. Jiang, C. Y. H. Chao, T. S. Zhao, *J. Power Sources* **2018**, *405*, 106–113; e) S. Liu, M. Kok, Y. Kim, J. L. Barton, F. R. Brushett, J. Gostick, *J. Electrochem. Soc.* **2017**, *164*, A2038-A2048.

[28] R. A. Elgammal, Z. Tang, C.-N. Sun, J. Lawton, T. A. Zawodzinski, *Electrochim. Acta* **2017**, *237*, 1–11.

[29] C. N. Sun, M. M. Mench, T. A. Zawodzinski, *Electrochim. Acta* **2017**, *237*, 199–206.

[30] X. L. Zhou, Y. K. Zeng, X. B. Zhu, L. Wei, T. S. Zhao, *J. Power Sources* **2016**, *325*, 329–336.

[31] U. S. D. o. Energy, **2009**, 70–70.

[32] a) C. Flox, M. Skoumal, J. Rubio-Garcia, T. Andreu, J. R. Morante, *Appl. Energy* **2013**, *109*, 344–351; b) J. Vázquez-Galván, C. Flox, C. Fàbrega, E. Ventosa, A. Parra, T. Andreu, J. R. Morante, *ChemSusChem* **2017**, *10*, 2089–2098.